Int. J. Nonlinear Anal. Appl. 13 (2022) 2, 1277–1295
ISSN: 2008-6822 (electronic)
http://dx.doi.org/10.22075/ijnaa.2022.6319

Performance investigation of a novel nature-inspired algorithm based maximum power point tracking controller for stand-alone PV Systems

Rinku Scaria[a,*], R. Neela[b], Bos Mathew Jos[c]

[a]Electrical and Electronics Department, Federal Institute of Science and Technology, Kerala, India

[b]Electrical Department, Annamalai University, Tamilnadu, India

[c]Electrical and Electronics Department, Mar Athanasius College of Engineering, Kerala, India

(Communicated by Javad Vahidi)

Abstract

A zero-emission photovoltaic system is critical for efficient energy supply and environmental protection. Because of the intermittent nature of solar insolation and temperature, the maximum power point tracking controller for the photovoltaic system has become complicated. At each intermittent condition, the photovoltaic array has only one operating point with maximum power output. Therefore, a nature-inspired algorithm-based controller is needed to determine the actual maximum operating point at different environmental conditions; thus, it can increase the overall efficiency of the photovoltaic system. This paper proposes a novel maximum power point tracking controller based on a hurricane optimization algorithm hybridised with chaos to improve power tracking in photovoltaic systems. The proposed hybrid algorithm is created by combining chaotic search behaviour with the standard hurricane optimization algorithm in order to increase efficiency. The proposed controller generates the optimal duty cycle for controlling the DC-DC boost converter by tracing the exact maximum operating point on a regular basis. The simulation results show that the proposed HOA -chaos-based MPPT controller outperforms INC, P& O, PSO and HOA based controllers in terms of efficiency and control.

Keywords: DC-DC boost converter, Hurricane optimization algorithm, Maximum power point tracking, Photovoltaic system, Chaos
2020 MSC: 65P20, 65K10, 76N25

1 Introduction

Renewable energy sources (RES) that utilize indigenous resources have the prospect to deliver electricity with nil or close nil greenhouse gases and air pollution. Moreover, the health benefits and environmental protection come from the growth of RES. Nowadays, the socio-economic benefits on the local economies are quite significant as a result of the power generation through RES rather than the traditional power generation methods. The developments in

*Corresponding author
Email addresses: rinkuscaria88@gmail.com (Rinku Scaria), neelaaueee@gmail.com (R. Neela), bosmathewjos@mace.ac.in (Bos Mathew Jos)

Received: February 2022 *Accepted:* March 2022

modern power plants bring significant socio-economic benefits in provincial economies, such as increased production, profits, local and regional employment. These socio-economic benefits increase job opportunities, salaries, and gross production either directly or indirectly.

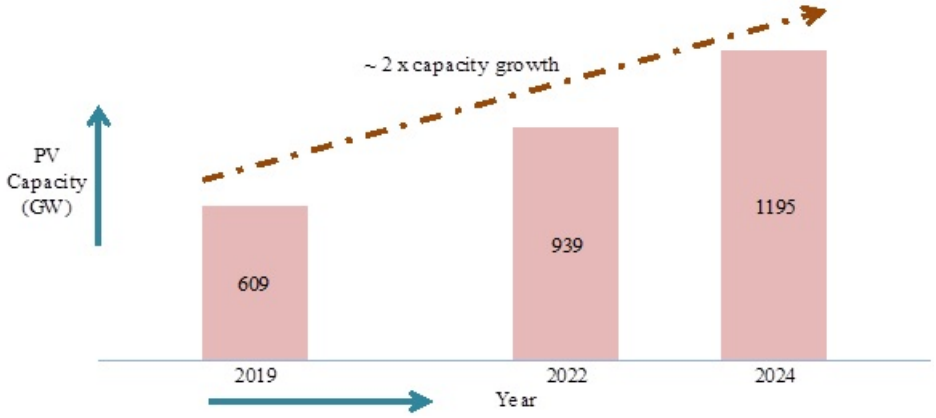

Figure 1: Cumulative global installed PV capacity

Among the RES, solar energy is ranked now at the upper end of the renewable energy list due to its availableness and more uniformly separated in nature than all other RES such as wind, hydro, tidal, and geothermal [12]. The earth receives more energy from the sun in just one hour than what humans consume in one year worldwide [23]. As per the investor overview presentation 2020 of First Solar, the global installed photovoltaic (PV) capacity is projected to double in the next five years from 609 GW to 1195 GW, as shown in Figure 1. The unsubsidized solar power sources have lower Levelized electricity costs (approximately 35 to 45 $/MWh) than the traditional power generations, such as coal-fired, nuclear, and gas-fired power plants, as shown in Figure 2. Concentrated solar power (CSP) provides the prospect of large-scale power production and comparatively low energy storage cost for base load power stations [2]. Currently, these applications reserve just 0.5% of the world's energy usage and are estimated to hit nearly 45% of the global energy consumption by 2050 [13]. At the beginning of 2014, a projection had made for the worldwide total installed capacity and annual power generation from the PV and CSP technologies. The total installed capacity was 3.93 GW for the CSP system and 191 GW for the PV system,which is assumed as the reference year for the 2050 forecast. The PV-CSP hybrid power station offers a viable electricity generation alternative in Northern Chile. It can efficiently satisfy the power demand of the mining industries in those regions [13].

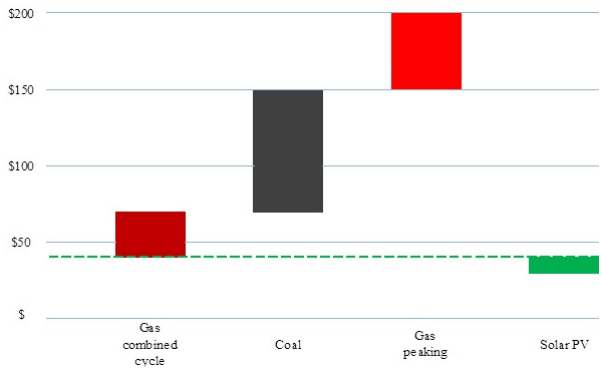

Figure 2: Levelized electricity cost

The PV array is usually known to have benign environmental consequences which do not produce chemical or noise pollution during electric power generation [9, 1]. It has proved most economical to use, as most devices need only a few power kilowatts in individual applications. It is one of the most feasible clean renewable energy solutions for urban usage, which substitutes conventional building cladding materials. It is also an enticing choice for national parks and scenic areas with the great benefit of preventing wires and pylons [24]. A solar PV home lighting system is used indomestic applications [6]. Solar energy is a typical and symbiotic alternative for pumping water systems [3]. It is one of the cheapest solar power applications with PV system direct drive,providing reliable services over several

decades [3]. PV solar cells installed on most modern satellites and illuminated by the sunlight provide the primary source of electricity for such satellites. The usage of renewable, regenerative solar energy from the PV array will best be recharged for the power supply in the batteries of the extended-range electric vehicles (EREV) [5].

Environmental temperature $T_{solar}$and the solar insolation IN_{solar} that fall on the PV array determine the amount of power produced by the PV cell. The main draw back in the PV power generation system is that the amount of power generated varies continuously due to the change in ambient temperature T_{solar} and solar in solation IN_{solar}.Because of these ever-changing atmospheric conditions, the PV array poses multiple local peak points on its P–V curve, which makes it more challenging for the PV system to identify the exact maximum power operating point (MPOP). Thus, an important factor in designing effective PV systems is the optimal finding of MPOP, which makes the maximum power point tracking (MPPT) more essential for the PV system to work optimally[10].An algorithm that hunts for the global maximum operating point based on the PV array voltage and current is the cornerstone for the MPPT controller.

Many scientists and programmers have successfully researched to monitor the MPOP of the PV module [15]–[8]. Lots of MPPT techniques for the PV system have been discussed in various literatures for the past two decades. are 19 distinct MPPT algorithms with some alterations in the existing MPPT algorithms that have been adopted [15]. These MPPT techniques differ in difficulty, precision, speed, MPOP oscillation, and the sensors'requirement to incorporate hardware. The literature demonstrates different methods to optimize PV power transmission to a variety of loads.Few researchers relied on selecting the characteristics of the PV array to match those load demands [8], while others altered the array setup (switching the PV array series-parallel connection) to fit the MPOP to satisfy the demands. The most widely employed MPPT techniques are hill climbing (HC), incremental conductance (INC),and perturbation and observation (P& O) algorithms [8]. The fixed iteration step-based P& O, INC, and HC approaches are comfortable and work well. Still, they are distinguished by a slow convergence, PV power oscillation across the MPOP, operation failure in ever-changing environmental temperatureT_{solar},and solar insolationIN_{solar}.The oscillations in finding the MPOP may be reduced by using the small perturbation step size;however,the tracking speed to find the MPOP is very slow [8]. Moreover, these standard MPPT techniques presume an approximate MPOP on the PV curve and may not assure the convergence to actual MPOP; instead,these techniques are always stuck in the local maximum since they cannot able to differentiate the actual global maximum.

The MPPT techniquesutilizing genetic algorithms (GA) and particle swarm optimization (PSO) with eagle strategy (ES) have been suggested to enhance the speed and preciousness of the MPOP tracking [8]. Furthermore, the statistical performance evaluation of the MPPT algorithms isbased on twenty modern meta heuristic algorithms such as GA, PSO, jay a algorithm (JA),firefly algorithm (FA), gravitational search algorithm (GSA), whale optimization algorithm (WOA), cuckoo search algorithm (CSA), sine cosine algorithm (SCA), multi-verse optimizer (MVO), radial movement optimization (RMO),imperialist competitive algorithm (ICA), antlion optimizer (ALO), mine blast algorithm (MBA), dragonfly algorithm (DFA), harmony search algorithm (HSA), water cycle algorithm (WCA), grey wolf optimizer (GWO), flower pollination algorithm (FPA), teaching learning-based optimization (TLBO), and differential evolution (DE)have been presented [16]. While they work well with the nonlinear features of I–V curves, they demand more computational time, and the flexibility of these algorithms is also restricted.In many PV power applications, neural networks and fuzzy controllers are employed totackle the nonlinearity in the I–V curve of the PV array [12, 23].

Most of these MPPT controllers are based on nature-inspired algorithms. The biggest challenge in real-time applications to use these algorithms is mainly related to different algorithm parameters. These are strongly nonlinear, dynamic, and stochastic parameters. The real challenges of optimizing the real-world mathematical problems are complex since they frequently require multiple variables and extremely nonlinear constraint and objective function. The scale and sophistication of the problems today need highly efficient optimization algorithms.

Moreover,all these methods estimate the approximate PV power transfer since they are related to particular ambient and load factors; a power loss occurs when these conditions are altered. To overcome the above disadvantages and achieve a rapid response speed, this paper proposes a rapid and precise MPPT technique based on a hurricane optimization algorithm (HOA) with chaos to extract the utmost power from the PV array panel.Note that the HOA-chaos has not historically been utilized in previous literature for the MPPT technique, which egresses as an analysis incentive that this paper aims to discuss. The HOA technique seeks to imitate the hurricane characteristics, the pressure profiles, and the radial wind. The HOA is being suggested as a heuristic candidate solution for large-scale NP-hard problems but has not been studied in PV applications. The HOA is recently viewed as a promising alternative algorithm to solve various problems in power systems and elastic optical networks [17]–[19]. The contributions of this paperer as follows:

(a) Presenting anaccurate and fast MPPT controller for the PV system based on the HOA and its variant by introducing chaotic dynamics.

(b) Applying the proposed HOA-chaos based MPPT controller to the PV system with a DC-DC boost converter to extract the utmost power from the PV array.
(c) Comparing the optimal results obtained from the PV system equipped with the proposed HOA-chaos based MPPT controller against the results of the PV system with the P&O, INC, PSO, and HOA based MPPT controllers independently.
(d) Analyzing the robustness and superiority of the proposed HOA-chaos based MPPT controller under various operating conditions such as solar insolation IN_{solar}variation and ambient temperature T_{solar}change.

The remainder of this paper is summarized as: the modeling and the fundamental equations of single diode PV cell and the practical PV array are shown in section 2. Section 3 describes the basic concepts of the hurricane and the mathematical formulation of the standard HOA algorithm. The theory and steps in the chaotic local exploration (CLE) are also presented in section 3. The execution of the proposed HOA-chaos based MPPT controller in the PV system is present in section 4, along with the algorithmic steps of the proposed HOA-chaos based MPPT controller on producing the maximum power from the PV cell.TheMATLAB simulation analysis and comparative results are depicted in section 5. Section 6concludes the overall benefits and superiority of the PV system with the proposed HOA-chaos based MPPT controller.

2 Modeling of PV Device

2.1 A. Modeling of Ideal PV Cell

The equivalent circuit of the single diode PV cellis depicted in Figure 3. The fundamental equation of the ideal PV cell from the semiconductor theory,which mathematically describes the I–V characteristic of PV cell, is expressed as [20],

$$I = I_{pv}^{cell} - I_0^{cell}\left[\exp\left(\frac{qV}{\underbrace{\alpha K}_{Id} T_{jun}}\right) - 1\right] \tag{2.1}$$

where I is the ideal PV cell net current; $I_{pv}^{cell}$is the current generated from the PV cell when the sunlight falls on it; I_0^{cell} is the diode leakage or reverse saturation current;$q = 1.60217646 \times 10^{-19}C$ represents the electron charge; V is the voltage across the terminal of the PV cell; α is the diode ideality constant; $k = 1.3806503 \times 10^{-23}J/K$ represents the Boltzmann constant.T_{jun} is the p–n junction temperature in Kelvin;represents the Shockley diode equation;

Figure 4 shows the I–V characteristic of an ideal PV cell derived from equation (2.1). As shown in Figure 4, the net PV cell current Iis the current difference between the solar-produced current and the current flowing through the diode I_d

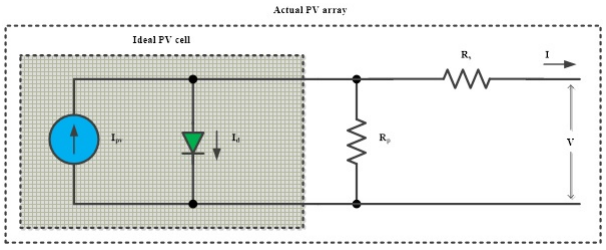

Figure 3: ActualPV array and ideal PV cell – Single diode model

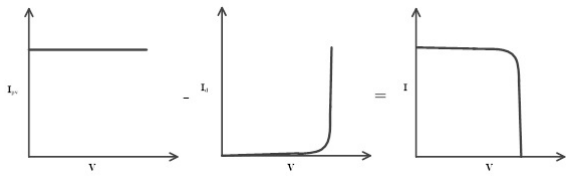

Figure 4: I–V Curveof an ideal PV cell

B. PV Array Modeling

The fundamental equation of the simple PV cell shown in (2.1) cannot show the real I–V curve of the actual PV array [20]. The actual PV array consists of multiple integrated cells. The visualization of the I–V characteristic at the PV array terminals requires the incorporation of additional parameters to the fundamental equation (2.1);thus, the equation of practical PV array can be written as [20],

$$I = I_{\text{pv}} - I_0 \left[\exp\left(\frac{V + R_s I}{V_t \alpha}\right) - 1\right] - \frac{V + R_s I}{R_p} \tag{2.2}$$

where, I_0 and I_{pv} are the array saturation current and PV current, respectively; $R_p$denotes the array's equivalent parallel resistance; R_s refers to the array's equivalent series resistance.

When the PV array consists of N_p parallel-connected cells, the saturation and PV currents of the array can be represented as,

$$I_0 = I_0^{\text{cell}} \times N_p \tag{2.3}$$

$$I_{\text{pv}} = I_{\text{pv}}^{\text{cell}} \times N_p \tag{2.4}$$

The thermal voltage V_t of the PV array modulewith N_s series-connected PV cells can be expressed as,

$$V_t = N_s kT/q \tag{2.5}$$

Series-connected cells give high terminal voltage, and parallel-connected cells result in a high current. Equation (2.2) depicts a practical PV array with a single diode model,as shown in Figure 3 [21]. The I–V characteristic of a practical PV cell shown in Figure 5 is originated from equation (2.2) which spotlights the three important points such as open circuit (V_{oc}, 0), MPOP (V_{MPOP}, I_{MPOP}), and short circuit (0, I_{sc}). In [4], to reflect the effect of carrier recombination, an additional diode is used. In [11], the effects of the three-diode model are given, which are not taken into account in the previous model. In order to make the diode model simple, the single diode is used in this paper, as depicted in Figure 3. In this paper, the Sun Power PV module is used for simulation studies and its parameters are shown in Table 1. Figure 6 and Figure 7 show the I–V and P–V characteristics of the SunPower PV module at 1000 W/m^2 solar insolation $IN_{solar}$with different temperature rangesT_{solar}(0°C, 25°C, and 50°C). The part number of Sun Power PV module used for the simulation analysis is SPR-305E-WHT-D.

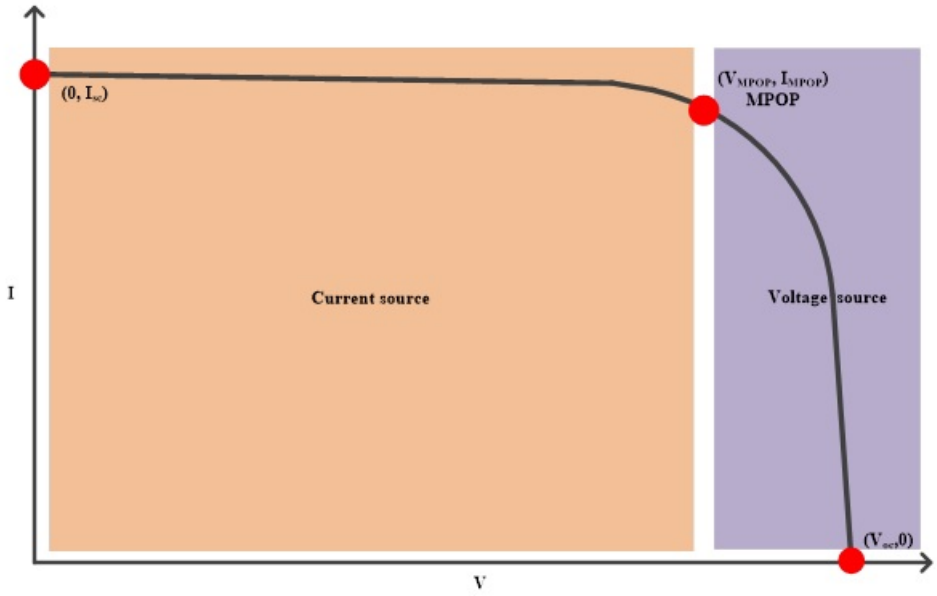

Figure 5: I–V characteristic with three outstanding points

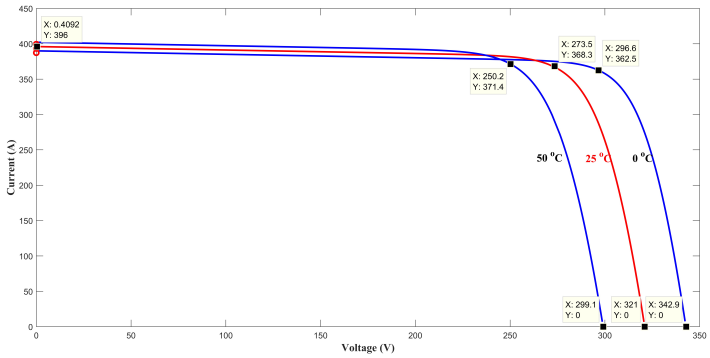

Figure 6: I–V characteristic of SPR-305E-WHT-D

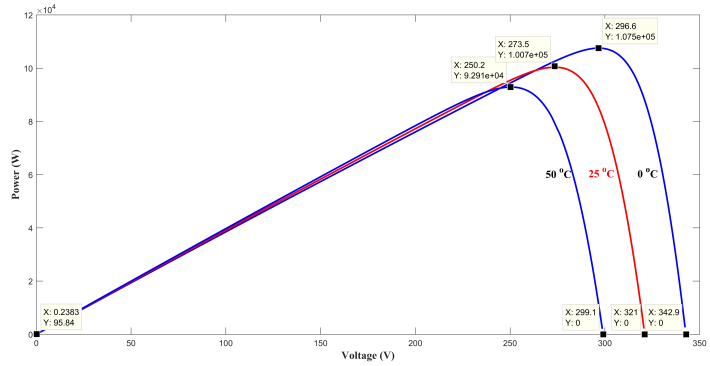

Figure 7: P–V characteristic of SPR-305E-WHT-D

3 Hurricane Optimization Algorithm with Chaos

A. Inside Hurricane

The low-pressure zone with a warm center developing over tropic and sub tropic oceans is called a hurricane [17, 18, 19]. The core of the hurricane is considered as the eye, as shown in Figure 8. The eye-wall is a region of mighty deep clouds and the most potent observed winds are situated just outside of the eye. Rain-bands are surrounding spiral bands that are the localized regions with strong winds,heavy rain, and deep clouds.

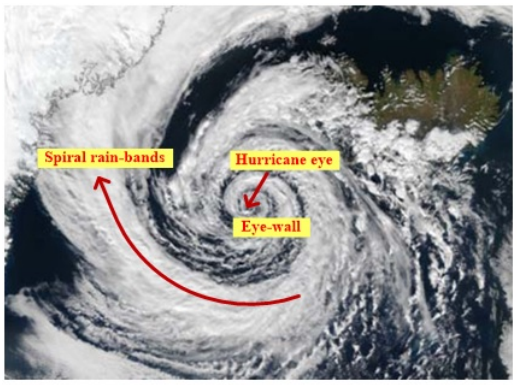

Figure 8: Inside a hurricane

The concept of the presented HOA algorithm is focused on hurricane observation and how the wind parcels travel through the surrounding environment.This phenomenon was modeled using several equations.The first provides a basic overview of the wind field.The model was first used by Depperman on hurricanes and defined as Rankine combined or modified Rankine vortex.

This vortex model is a basic definition of two parametric equations describing the swirl flow. The flow is solidly rotated in the internal radial regions around the center, while the outside is vortex free.

$$W = W_{max}\frac{r}{Rw_{max}} \qquad if \quad r < Rw_{max} \tag{3.1}$$

$$W = W_{max}\left(\frac{r}{Rw_{max}}\right)^{s} \qquad if \quad r > Rw_{max} \tag{3.2}$$

where,

Wdenotes the tangential wind whenr = $\mathrm{Rw_{max}}$;

$\mathrm{W_{max}}$ is the maximum value of tangential wind;

$\mathrm{Rw_{max}}$ is the radius of the wind at maximum speed in the range of 0 to + ∞;

sis a scaling parameter that may be adjusted to suit available data in the regionof the wind field outside of $\mathrm{Rw_{max}}$.

This model is used by the proposed approach to control velocity shift over the exploration space.In a hurricane, the interaction of the external factors is forcing the wind parcel to start to spiral outwards. Thus, a spiral logarithmic pattern can approximate the high horizontal surface of the hurricane. The logarithmic spirals may be represented as,

$$x(\theta) = r(\theta)\cos\theta + e_x \tag{3.3}$$

$$r(\theta) = a\exp(b.\theta) \tag{3.4}$$

$$y(\theta) = r(\theta)\sin\theta + e_y \tag{3.5}$$

where a is a real number that is greater than 0;(x, y) is the location in Cartesian coordinates;$\mathrm{e_x}$and$\mathrm{e_y}$are the real numbers that represent the coordinates of the eye; θ and r are angular and radial coordinates in polar coordinates;bassures how closely and in what direction the spiral whirls. The spiral transforms into a circle with radius $a\ if\ b = 0$.

The lower pressure (eye) represents the optimal solution of the HOA algorithm. The eye pressure is calculated by using the objective function of the optimization problem.

B. Standard Hurricane Optimization Algorithm

Let us consider a problem search space with S parcels (population size). Thus, the location of the $\mathrm{i^{th}}$ parcel $\mathrm{H_i}$ can be expressed as,

$$H_i = \left(h_i^1, h_i^2, \ldots, h_i^d\right) \qquad for\ i = 1, 2, \ldots, S \tag{3.6}$$

where d is the dimension of the problem.

The wind parcels Hare split into j groups,i.e., each parcel , here. For the parcel ,starts from the eye location (optimal solution),the $\mathrm{j^{th}}$ dimension of the$\mathrm{i^{th}}$ parcel $\mathrm{H_i}$ is computed as,

$$h_i^j = \begin{cases} r_i(t).\sin(\phi_{i,initial} + \phi_i(t)) + e^j & if \quad j = k+1 \\ r_i(t).\cos(\phi_{i,initial} + \phi_i(t)) + e^j & if \quad j = k \\ e^j & else \end{cases} \tag{3.7}$$

$$r_i(t) = Rw_0.\exp(\phi_i(t).rand) \tag{3.8}$$

where ϕ_i and r_i are angular and radial coordinates in polar coordinates; e^j denotes the value of the eye (optimal solution) on $\mathrm{j^{th}}$ dimension;tis the iteration count; At $t = 0$, $r_i(0) = Rw_0$ and $\phi_i(0) = 0$. In other words, at $t = 0$, $\phi_{i,initial}$ *and* Rw_0 are the initial polar coordinates, as shown in Figure 9, Rw_0 is the eye radius in the range of 0 to $+\infty$. The values $\phi_{i,initial}$ for $i = 1, 2, 3, \ldots, S$ is arbitrarilyinitializedin the range of 0 to 2π; rand is a random number in the range of 0 to 1.

Every parcel travels along the spiral paths in the are constituted by the 2-dimensionalk and k+1. The parcel requires velocity to begin and continue to move. Hence, the parcel velocity $\mathrm{H_i}$ is conceived as the angular velocity, i.e.,rate of change of angular displacement summed with its angular coordinate ϕ_i.

$$\begin{cases} \phi_i(t+l) = \phi_i(t) + \omega & if\ r_i \le R\omega_{max} \\ \phi_i(t+l) = \phi_i(t) + \omega.\left(\frac{Rw_{max}}{r}\right)^{rand} & if\ r_i > Rw_{max} \end{cases} \tag{3.9}$$

where ω is the angular velocity defined in the range of 0 *to* 2π, Under the condition $Rw_0 < Rw_{max}$,rand is a uniformly distributed random variable in the range of 0 to 1;

For every iteration, the parcel alters its location. In the minimization problem, the eye travels to the parcel location to hold the low pressure (optimal solution) at the eye if $F_i < F_{eye}$, whereas in the maximization problem, the eye travels to the parcel location if $F_i > F_{eye}$.F_i and F_{eye}can be expressed as,

$$F_i = fit_i = f\left(h_i^1, h_i^2, \ldots, h_i^d\right) \tag{3.10}$$

$$F_{eye} = \begin{cases} \min\left(fit_i(t)\right) & for \;\; i = 1, 2, \ldots, S; \quad \text{if problem is minimization} \\ \max\left(fit_i(t)\right) & for \;\; i = 1, 2, \ldots, S; \quad \text{if problem is maximization} \end{cases} \tag{3.11}$$

where $fit_i(t)$denotes the objective function of the parcel H_i at t^{th} iteration.

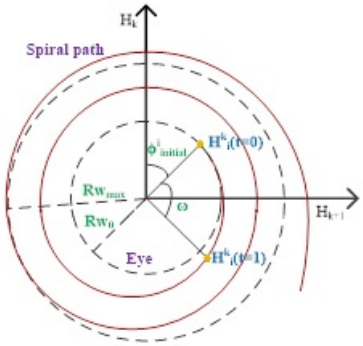

Figure 9: Different parameters (green) and variables (blue) of HOA

C. Chaotic Local Exploitation(CLE)

Chaotic dynamics are integrated into the basic HOA technique to improve quest efficiency and prevent getting stuck into a local minimum or maximum[7]. Chaos is a type of nonlinear system's characteristics; it is a bounded unstable complex action with a sensitive reliance upon initial conditions and an infinite amount of unstable periodic movements.Even though it tends to be stochastic, it does exist under deterministic situations in the nonlinear deterministic systems.The development of interests in physics, chemistry, biotechnology, and engineering has recently prompted studies of the chaos to be controlled, synchronized, and optimized[7]–[25].Thanks to its simple functioning and the unique capacities to prevent getting stuck at local maximum or minimum, a chaos-based searching technique has become a modern optimization strategy [7].

In this paper, the chaotic logistic equation is used to build the HOA-chaos, revealing the sensitive dependency of initial conditions[7]. The logistic equation of chaos for local exploration can beexpressedas,

$$ch^j(tc+1) = \mu.ch^j(tc)(1 - ch^j(tc)) \quad for \;\; j = 1, 2, \ldots, d\,; \;\; 0 \le ch^j(0) \le 1 \tag{3.12}$$

where ch^j is the j^{th}chaotic variable which is distributed in the range 0 to 1;μ is the chaos control parameter;tc is the iteration count of CLE.

Even though the equation (17) is deterministic, it shows chaos dynamic when $\mu = 4$ and ch(0){0, 0.25, 0.5, 0.75, 1}[7]. There is a reasonable change in the long-time character of chaos, even for a small difference in its initial value. The direction of the chaotic variable will move through the entire exploration space ergodically. Generally, the chaotic variable has unique properties such as irregularity, pseudo-randomness, and ergodicity. The procedures of CLE are explained as follows,

Step 1: Set $tc = 0$, and map the optimal solution $H_g(tc)$ with the decision variable $\left[h^1(tc+1), h^2(tc+1), \ldots, h^d(tc+1)\right]$ in the limitsfor $j = 1, 2, 3, .., d$ to the chaotic variable $ch^j(tc)$ in the range of $[0, 1]$ as,

$$ch^j(tc) = \frac{h^j(tc) - h^j(tc)_{min}}{h^j_{max} - h^j_{min}} \quad for \quad j = 1, 2, \ldots, d \tag{3.13}$$

Step 2: For j = 1,2,3,..,d, compute the chaotic variablech^j(tc+1)for the next iteration tc+1using the chaos logistic equation (3.12).

Step 3: For j = 1,2,3,..,d, convertthe chaotic variable ch^j(tc+1)to decision variables h^j(tc+1)as,

$$h^j(tc+1) = h^j_{min} + ch^j(tc)\left(h^j_{max} - h^j_{min}\right) \quad for \quad j = 1, 2, \ldots, d \tag{3.14}$$

Step 4: Calculate the fitness value F_g(tc+1)for the new feasible solution H_g(tc+1),with the decision variables [h^1(tc+1),h^2(tc+1),h^3 . . . ,h^d(tc+1)] updated using chaotic dynamics.

Step 5: Check whether the new solution H_g(tc+1)is better than the previous optimal solution H_g(tc)or the specified maximum number of iterationstc_{max} is achieved?If yes, update the new optimal solution as the optimal output of the CLE; else, settc = tc + 1 and go to step 2.

D. Proposed HOA with Chaos

Based on the presented HOA and the CLE, a two-phased hybrid algorithm named HOA-chaos is proposed. HOA is employed to execute the global exploration, and CLE is incorporated to execute the local exploitation for the optimal solution obtained from the HOA. The HOA technique is employed for exploration by globally modifying the variables, and the ergodic chaos dynamic is utilized for local exploitation by updating the optimal solution obtained from the HOA.In addition, multiple new solutions are spontaneously generated and introduced into the new population to preserve population diversity.Remarkably, the area for generating a new feasible solution is dynamically diminished to speed up convergence.The area in particular to produce new solutions is dynamically diminished to accelerate the algorithm's convergence characteristics.

4 HOA-Chaos based MPPT Controller for PV System

A. Test System

It is appropriate to connect a DC-DC boost converter directly to the PV array to execute the MPPT algorithm. The circuit configuration of the DC-DC converter employed in the presented work is the typical step-up boost converter,as depicted in Figure 10. The theory and principleof the step-up boost converter are popularly established in the literature[15].The specification of the PV panel Sun Power SPR-305E-WHT-D and DC-DC boost converter are depicted in Table 1.

Table 1: PV system specification

Symbol	Parameter	Value	
	DC-DC boost converter		
P_{rated}	Rated power	100	kW
f_s	Switching frequency	5	kHz
C_{in}	Converter input capacitor	100	uF
L_{in}	Converter input inductance	5	mH
C_{out}	Converter output capacitor	100	mF
R_L	Load resistance	1	ohm
	Solar panel - SunPower SPR-305E-WHT-D		
P_{MPOP}	Maximum Power	305	W
I_{sc}	Short-circuit current	5.96	A
I_{MPOP}	Current at MPOPat 25 °C	5.58	A
V_{oc}	Open-circuit voltage	64.2	V
V_{MPOP}	Voltage at MPOPat 25 °C	54.7	V
N_{cell}	Cells per module	96	no
N_{par}	Parallel strings	66	no
N_{ser}	Series-connected modules per string	5	no
T_s	Sampling time – MATLAB model	1 x 10^{-6}	

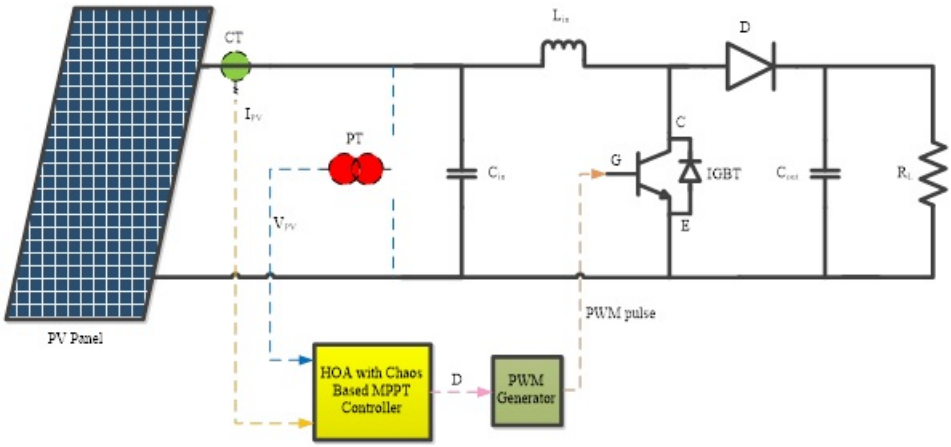

Figure 10: PV system consists of DC-DC boost converter, HOA-chaos based MPPT controller, and PVpanel

B. Fitness Function

The primary goal of the HOA-chaos based MPPT controller is to identify the optimal duty cycle$D_{optimal}$ of DC-DC boost converter that can extracts maximum PV power P_{MPOP}(i.e.,optimal PV voltage V_{MPOP} and optimal PV current I_{MPOP}) from the PV array at any level of solar insolation $IN_{solar}$and temperatureT_{solar}. Thus, the decision variable of the HOA-chaos based MPPT controller is the duty cycle D. Hence, the fitness function (fitness value of the wind parcel) of the proposed HOA-chaos based MPPT controller can be expressed as,

$$Max\ P_{PV}(D) = V_{PV} \times I_{PV}(D) \tag{4.1}$$

$$P_{MPOP} = V_{MPOP} \times I_{MPOP} \tag{4.2}$$

where I_{PV}(D)and V_{PV}(D)are the current and voltage measured from the PV array when the DC-DC boost converter works at a duty cycle D; and are the measured PV voltage and PV current correspond to the boost converter operates at optimal duty cycle $D_{optimal}$.

Table 2: Parameters of HOA-chaos

Symbol	Parameter	Value
S	Number of parcels	10
d	Problem dimension	1
Rw_{max}	Radius of the maximum wind speed	0.2
Rw_0	Eye radius	1 x 10^{-5}
ω	Wind angular velocity	$\pi/10$
µ	Control parameter	4
t_{max}	Maximum number of iterations - HOA	100
tc_{max}	Maximum number of iterations - Chaos	10
D_{min}	Duty cycle lower limit	0.05
D_{max}	Duty cycle upper limit	0.9
$D_{initial}$	Initial duty cycle	0.5

C. Algorithmic Steps in the Proposed HOA-Chaos Based MPPT Controller

The proposed HOA-chaos-based MPPT controller's output argument is a duty cycle D within the range [0, 1].Thealgorithmic steps in the proposed HOA-chaos based MPPT controller are discussed as follows,

Step 1: Read MPPT controller variables, HOA and chaos parameters such as the number of parcels, S; problem dimension, d; the radius of the maximum wind speed, Rw_{max}; eye radius, Rw_0; angular velocity, ω; control parameter, μ; the maximum number of iterations for HOA and chaos, t_{max} and tc_{max} respectively; duty cycle range ; initial duty cycle $D_{initial}$;and the sampling time T_s of MATLAB simulation model.The values of all these parameters are given in Table 1 and 2.

The proposed HOA-chaos-based MPPT controller generates the initial duty cycle Dinitial to function the PV system's DC-DC boost converter at the beginning of the MATLAB simulation.

Step 2:For i = 1, 2, 3, ..., S, arbitrarily generate the values of $\phi_{i,initial}$ in the range of 0 to 2π.

Step 3: Set t = 0 and randomly assume initial location for eye H_{eye} within the interval as,

$$H_{eye} = \left[e^1, e^2, \ldots, e^d\right] \tag{4.3}$$

$$e^j = h^j_{min} + rand.\left(h^j_{max} - h^j_{min}\right) \quad for \;\; j = 1, 2, \ldots, d \tag{4.4}$$

In this proposed MPPT controller, d = 1, thus =. Therefore, the location of eye is written as,

$$H_{eye} = [e] \tag{4.5}$$

$$e = h_{min} + rand.\,(h_{max} - h_{min}) \tag{4.6}$$

Step 4:At this instant, the proposed MPPT controller outputs the duty cycle e to operate the DC-DC boost converter and the corresponding voltage $V_{PV}(e)$ and current $I_{PV}(e)$ are measured. Further, inside the MPPT controller, the fitness value F_{eye} of the eye H_{eye} is computed using PV power equation (4.1) as,

$$F_{eye} = V_{PV}(e) + I_{PV}(e) \tag{4.7}$$

Step 5:Divide all wind parcels $H_{(i\,=\,1,2,..,S)}$ into j groups ($j = d - 1$), such that each parcel $H_i \in G_k$, where $k = i \;\; mod(d-1)$.

In this proposed MPPT algorithm, j = 1 - 1 = 0, hence all wind parcels are grouped together.

Step 6:For i = 1, 2, 3, ..., S,calculate the feasible location for parcel H_i using equation (12). If any of the decision variables in H_i violate the limits $\left[h^j_{min}, h^j_{max}\right]$, then randomly generate the values of $\phi_{i,initial}$ in the range of 0 to 2π, set $\phi_i = 0$, and the violated variables can be bounded within limits as,

$$h^j = \begin{cases} h^j_{min} & if \quad h^j < h^j_{min} \\ h^j_{max} & if \quad h^j > h^j_{max} \end{cases} \tag{4.8}$$

In MPPT controller application, since the dimension of the problem is d = 1, the equation (4.8) is written as,

$$h = \begin{cases} D_{min} & if \quad h < h^j_{min} \\ D_{max} & if \quad h > h_{max} \end{cases} \tag{4.9}$$

Step 7:For every instant i = 1 to S,the controller outputs the duty cycle h_i to operate the DC-DC boost converter and the corresponding voltage $V_{PV}(e)$ and current $I_{PV}(e)$ are measured. Further, inside the MPPT controller, the fitness value F_i of the parcel $H_i$is calculated using equation (4.1) as,

$$F_i = v_{PV}(h_i) \times I_{PV}(h_i) \tag{4.10}$$

Step 8:Find the best fitness value F_{best} among all parcels. If $F_{best} > F_{eye}$, then $F_{eye} = F_{best}$ and update the location of the eye H_{eye} with the best parcel H_{best}. Such that, H_{eye} is the optimal duty cycle $D_{optimal}$ at this instant. Thus, the MPPT controller generates the optimal duty cycle H_{eye} to operate the DC-DC boost converter with maximum power at this instant.

Step 9:Employ CLE on the best parcel H_{eye}. Set $H_g = H_{eye}$ and $F_g = F_{eye}$, alter the location of the best parcel H_g using equations (18) and (19).Update the location of the eye H_{eye} with the optimal parcel's location H_g obtained from the CLE if the fitness value F_g of CLE parcel is better than the eye pressure F_{eye}.

Step 10:Set t = t + 1, for i = 1, 2, 3, ..., S,update the angular coordinate ϕ_i with the angular velocity ω using equation (3.9).

Step 11:Check whether the maximum number of iterationt_{max} is reached, i.e., $t > t_{max}$?If yes, output the location of eye H_{eye} as the optimal result of the proposed HOA-chaos algorithm, i.e., the MPPT controller generates the optimal duty cycle H_{eye} to operate the DC-DC boost converter with global maximum power P_{MPOP};else go to step 6.

5 Simulation Analysis

In this paper, the switching frequency f_s of the DC-DC boost converter is chosen as 5 kHz. Irrespective of solar insolation IN_{solar} and temperature T_{solar} variations, the steady-state and transient responses of the PV power generation system also depend on the system parameters and converter topology. Therefore, in order to assess the HOA-chaos based MPPT controller with the conventional P&O, INC, PSO, and HOA based MPPT controllers, all these controllers are implemented independently on a PV system with the same parameters and DC-DC converter topology. The PV system equipped with each of the presented MPPT controllers is examined and verified through the simulation model in the MATLAB Simulink environment.

The MATLAB simulation model of the PV system with these MPPT controllers is simulated for t_{sim} = 6 s; in which the steady-state performance of the PV system is analyzed during 0 s to 1.5 s; and its transient performance is analyzed during 1.5 s to 6 s.In the transient performance analysis, three different scenarios are considered: solar insolation IN_{solar}variation, temperature T_{solar}variation, and simultaneous variation. The steady-state and transient behaviors of PV terminal voltage V_{PV} and load voltage V_{Load} are shown in Table 3. The average power P_{PVavg}generated from the PV array and the average power $P_{Loadavg}$consumed by the resistive load $R_L$for all the four MPPT controllers are compared in Table 4.

A. Steady-State Performance (t_{sim} = 0 s to 1.5 s)

Figure 11 shows the steady-state response of power P_{PV} extracted from the PV panel, PV terminal voltageV_{PV}, and current $I_{PV}$with respect to constant solar insolation IN_{solar}(1000 W/m^2) and temperatureT_{solar}(25 °C). From Figure 11, it is seen that the PV terminal voltage $V_{PV}$of the PV system with the INC based MPPT controller took more time to settle with t_{settle} of 0.5795 s. Whereas the PV terminal voltage $V_{PV}$of the PV system with the P&O based MPPT controller took0.3091 s to settle, but lesser than that of the INC based MPPT controller.Meanwhile, the PV terminal voltage $V_{PV}$of the PV system with the presented metaheuristic (PSO, HOA, and HOA-chaos) algorithms based MPPT controllers settled much quicker than that of the traditional (INC and P&O) MPPT controllers with $t_{settle}$of 0.3058s for PSO, 0.3049s for HOA, and 0.3030sfor HOA-chaos, as shown in Table 3.

Although the PV terminal voltage $V_{PV}$of the PV system with the presented MPPT controllers except INC based controller does not have any undershoot under steady-state condition, the PV terminal voltage V_{PV} has an overshoot of 0.5681 % for P&O, 8.4307 % for INC, 0.4012 % for PSO, 0.3057 % for HOA, and 0.3032 %for HOA-chaos based MPPT controller. Thus, by seeing the metrics such as settling time t_{settle}, percentage overshoot, and percentage undershoot of the PV terminal voltage V_{PV} in Table 3 and Figure 11, it is evident that the PV system with the proposed HOA-chaos based MPPT controller responded much faster than that of the other presented MPPT controllers, with very low oscillations on the PV terminal voltage V_{PV}.

It is widely known that the supreme aim of the MPPT controller is to extract the maximum power from the PV array. Therefore, the power P_{PV}extracted from the PV array for each of the presented MPPT controllers needs to be compared together to determine which technique extracted the maximum power. Thus, the waveform of PV output power $P_{PV}$of the PV system with each of the presented MPPT controllers are taken for the comparison to show which one extracted the maximum power from the PV array. Table 4 shows the comparison of average PV output power P_{PVavg} and the average power$P_{Loadavg}$ delivered to the load R_L of the PV system with each of the presented MPPT controllers. From Table 4, it is seen that the PV system with the proposed HOA-chaos based MPPT controller extracted the maximum average power $P_{PVavg}$of 94.1907 kW under constant solar insolation IN_{solar}(1000 W/m^2) and temperature T_{solar}(25 °C)during 0 s to 1.5 s. In contrast,the PV system equipped separately with the P&O, INC, PSO, and HOA based MPPT controllers extracted merely 83.5319 kW, 71.7857 kW, 89.9359 kW, and 91.6491 kW of average power $P_{PVavg}$from the PV array, respectively, as shown in Table 4.

Figure 12 shows the steady-state response of voltageV_{Load}across the resistive load R_L, powerP_{Load}, and current I_{Load} consumed by the resistive load $R_L$with respect to constant solar insolation IN_{solar}(1000 W/m^2) and temperatureT_{solar}(25 °C). As like the wave form of PV terminal voltage V_{PV}in Figure 11, the voltage V_{Load}waveform across the resistive load $R_L$in Figure 12 shows that the PV system with the INC based MPPT controller took more time to settle with $t_{settle}$of 0.6235s. The load voltage $V_{Load}$of the PV system with the P&O based MPPT controllergot settled at 0.3117 s, but lesser than that of the INC based MPPT controller.The load voltage $V_{Load}$of the PV system with the PSO, HOA, and HOA-chaos based MPPT controllers got settled at 0.3079s, 0.3071s, and 0.3048s, respectively. Thus, it is seen that the steady-state response characteristic of the load voltage V_{Load}forthe PV system with the proposed HOA-chaos based MPPT controller is much better than that of the other presented MPPT controllers in terms of settling time t_{settle}, percentage overshoot, and percentage undershoot. As a whole, Table 3 shows the rise

timet$_{\text{rise}}$, settling timet$_{\text{settle}}$, percentage overshoot, and percentage undershoot of both PV terminal voltageV$_{\text{PV}}$ and load voltageV$_{\text{Load}}$under steady-state condition.

From Figure 12 and Table 4, it is seen that the PV system with the proposed HOA-chaos based MPPT controller delivered the power P$_{\text{Loadavg}}$to the load R$_{\text{L}}$ at an average of 90.7264 kWduring 0 s to 1.5 s; whereas the same PV system equipped with individual P&O, INC, PSO, and HOA based MPPT controllers delivered79.5515 kW, 69.1516 kW, 86.5621 kW, and 88.333 kWpower P$_{\text{Loadavg}}$to the load R$_{\text{L}}$, respectively. Therefore from Figure 11 and Figure 12, it can be concluded that the PV system with the proposed HOA-chaos based MPPT controller extracted the maximum power P$_{\text{PV}}$ from the PV array and then delivered the utmost power P$_{\text{Load}}$ to the load R$_{\text{L}}$ as compared to the same PV system equipped with the other presented MPPT controllers individually.

Table 3: Steady-state and dynamic responses of PV voltage and load voltage

State	*Simulation time(s)*	*MPPT Controller*	*Signal*	*Rise time, $t_{rise}(s)$*	*Settling time, $t_{settle}(s)$*	*Overshoot(%)*	*Undershoot(%)*
Steady-state	$0 < t_{sim} < 1.5$	*P&O*	V_{PV}	*0.1728*	*0.3091*	*0.5681*	*0*
		INC		*0.4413*	*0.5795*	*8.4307*	*13.1074*
		PSO		*0.1718*	*0.3058*	*0.4012*	*0*
		HOA		*0.1713*	*0.3049*	*0.3057*	*0*
		HOA-Chaos		*0.1702*	*0.3030*	*0.3032*	*0*
		P&O	V_{Load}	*0.1893*	*0.3117*	*0.0327*	*0*
		INC		*0.4672*	*0.6235*	*0.0315*	*0*
		PSO		*0.1879*	*0.3079*	*0.0162*	*0*
		HOA		*0.1870*	*0.3071*	*0.0148*	*0*
		HOA-Chaos		*0.1851*	*0.3048*	*0.0139*	*0*
	$1.5 < t_{sim} < 3$	*P&O*	V_{PV}	-	-	*7.7956*	*38.2522*
		INC		-	-	*9.3528*	*44.5199*
		PSO		-	-	*7.6305*	*35.8988*
		HOA		-	-	*7.1748*	*33.211*
		HOA-Chaos		-	-	*5.9373*	*17.8603*
		P&O	V_{Load}	-	-	*0.0577*	*0*
		INC		-	-	*0.0267*	*0*
		PSO		-	-	*0.0242*	*0*
		HOA		-	-	*0.019*	*0*
		HOA-Chaos		-	-	*0.015*	*0*
Transient	$3 < t_{sim} < 4.5$	*P&O*	V_{PV}	-	-	*1.6033*	*0*
		INC		-	-	*2.8749*	*0*
		PSO		-	-	*1.3693*	*0*
		HOA		-	-	*1.3279*	*0*
		HOA-Chaos		-	-	*1.2989*	*0*
		P&O	V_{Load}	-	-	*0.15*	*0*
		INC		-	-	*0.197*	*0*
		PSO		-	-	*0.149*	*0*
		HOA		-	-	*0.0172*	*0*
		HOA-Chaos		-	-	*0.01329*	*0*
	$4.5 < t_{sim} < 6$	*P&O*	V_{PV}	-	-	*7.6649*	*36.7087*
		INC		-	-	*7.8361*	*34.586*
		PSO		-	-	*7.6093*	*32.5281*
		HOA		-	-	*7.5261*	*23.1034*
		HOA-Chaos		-	-	*5.8978*	*7.9742*
		P&O	V_{Load}	-	-	*0.0194*	*0*
		INC		-	-	*0.0168*	*0*
		PSO		-	-	*0.0165*	*0*
		HOA		-	-	*0.015*	*0*
		HOA-Chaos		-	-	*0.0135*	*0*

B. Transient Performance

The dynamic behavior of the PV system with the presented MPPT controllers (P&O, INC, PSO, HOA, and HOA-chaos) is investigated in dividedly under three different operating conditions, namely solar insolation IN$_{\text{solar}}$variation,

Table 4: Comparison of average PV power and the average power consumed by the load

State	*Simulation time(s)*	*MPPT Controller*	*Average solar insolation falls on PV panel, $IN_{solar}(W/m^2)$*	*Temperature, $T_{solar}(^oC)$*	*Average power extracted from the PV panel, $P_{PVavg}(kW)$*	*Average power utilized by the resistive load, $P_{Loadavg}(kW)$*
Steady-state	$0 < t_{sim} < 1.5$	*P&O*	*1000*	*25*	*83.5319*	*79.5515*
		INC			*71.7857*	*69.1516*
		PSO			*89.9359*	*86.5621*
		HOA			*91.6491*	*88.333*
		HOA-Chaos			*94.1907*	*90.7264*
	$1.5 < t_{sim} < 3$	*P&O*	*933.33*	*25*	*83.4184*	*82.5375*
		INC			*85.0618*	*84.449*
		PSO			*85.3413*	*84.986*
		HOA			*88.1331*	*87.7232*
		HOA-Chaos			*90.3527*	*89.7158*
Transient	$3 < t_{sim} < 4.5$	*P&O*	*1000*	*33.33*	*87.8406*	*86.3925*
		INC			*89.8499*	*88.7364*
		PSO			*93.1014*	*92.3743*
		HOA			*93.7312*	*93.1199*
		HOA-Chaos			*97.1976*	*96.5193*
	$4.5 < t_{sim} < 6$	*P&O*	*933.33*	*33.33*	*81.4521*	*80.7888*
		INC			*82.7162*	*82.3048*
		PSO			*85.2257*	*84.8715*
		HOA			*87.7175*	*87.3235*
		HOA-Chaos			*90.2503*	*89.6143*

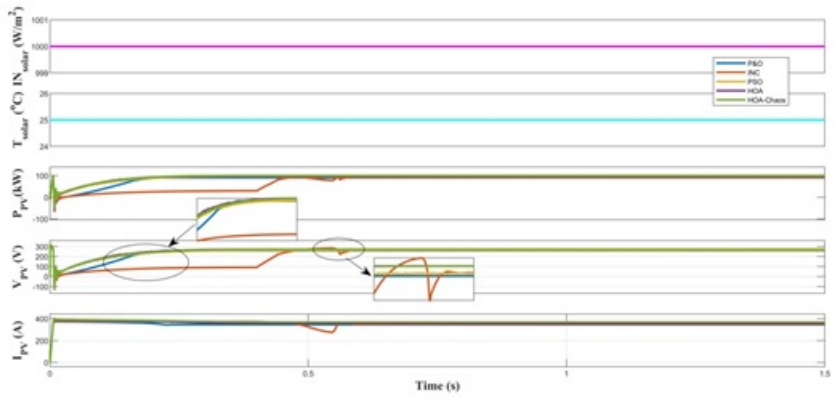

Figure 11: Steady-state response – PV output powerP_{PV}, terminal voltageV_{PV}, and currentI_{PV}

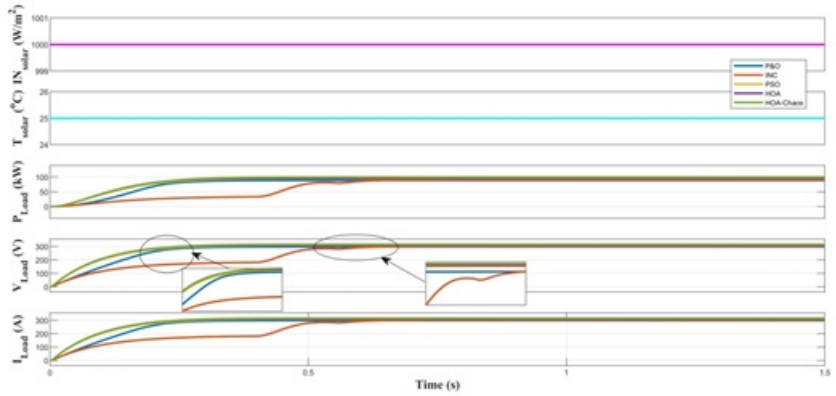

Figure 12: Steady-state response – Load powerP_{Load}, voltageV_{Load}, and currentI_{Load}

temperature T_{solar}variation, and simultaneous variation of both insolation $IN_{solar}$and temperatureT_{solar}.

Scenario 1 – Considering solar insolation variation(t_{sim} = 1.5 s to 3 s)

In this scenario, the simulation waveforms during1.5 s to 3 s are taken for the analysis. The solar insolation IN_{solar}falls on the PV array is considered as 1000 W/m^{2}during1.5 s to 2 s; then it is stepped down to 800 W/m^2 at 2 s and maintained constant until2.5 s; further, it is stepped up to 1000 W/m^{2}at 2.5 s and maintained constant until3 s. In the meantime, the temperature $T_{solar}$is maintained constant at 25 °C.

during 1.5 s to 3 s with respect to change in solar insolation IN_{solar}. Table 4 and Figure 13 show that the PV system with the proposed HOA-chaos based MPPT controller extracted the maximum average power of 90.3527 kWduring 1.5 s to 3 s. Whereas the PV system with the P&O, INC, PSO, and HOA based MPPT controllers extracted merely 83.4184 kW, 85.0618 kW, 85.3413 kW, and 88.1331 kW, respectively.

Figure 14 shows the response of load power P_{Load}, load voltage V_{Load}, and load current I_{Load}during 1.5 s to 3 s with respect to change in solar insolationIN_{solar}. From Figure 14 and Table 4, it is seen that the PV system with the HOA-chaos based MPPT controller exported the maximum average power of 89.7158 kW to the load, whereas the PV system with the P&O, INC, PSO, and HOA based MPPT controllers exported 82.5375 kW, 84.449 kW, 84.986 kW, and 87.7232kW, respectively. Whenever the solar insolation varies, the load power P_{Load}, load voltage V_{Load}, and load current I_{Load}waveforms for the PV system with the presented P&O, INC, PSO, and HOA based MPPT controllers are shown more oscillations. In contrast, the load powerP_{Load}, load voltage V_{Load}, and load current I_{Load}waveforms for the PV system with the proposed HOA-chaos based MPPT controller responded quickly and settled with very minimum oscillation.

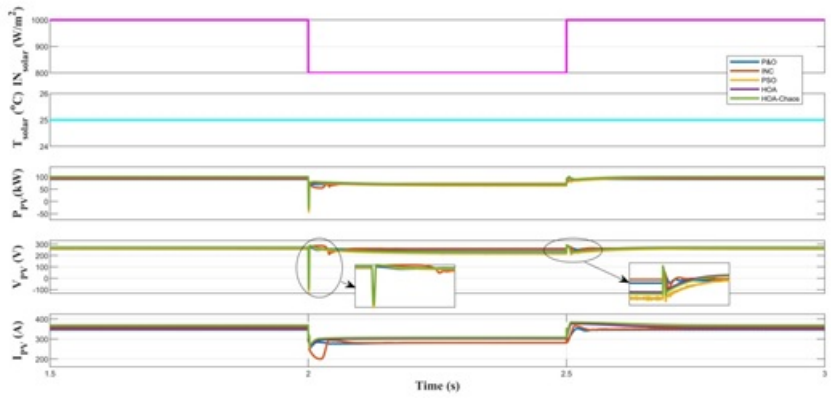

Figure 13: shows the response of PV output powerP_{PV}, PV terminal voltageV_{PV}, and current I_{PV}

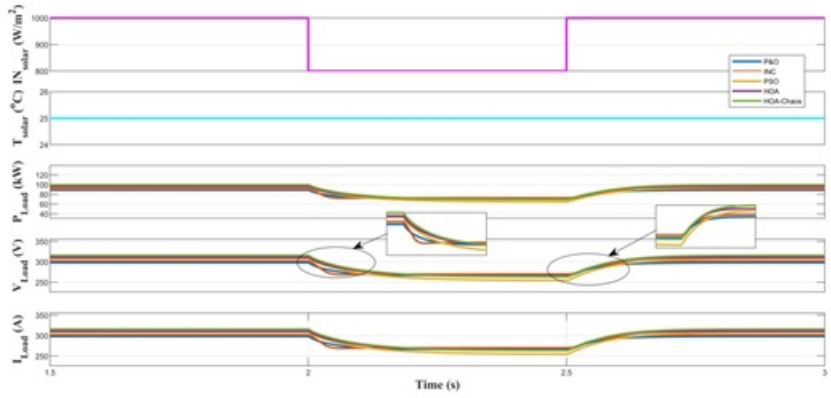

Figure 14: Scenario 1 – Load power P_{Load}, voltage V_{Load}, and current I_{Load}

Scenario 2 – Considering temperature variation(t_{sim} = 3 s to 4.5 s)

In this scenario, the solar insolation IN_{solar}that falls on the PV array is assumed as constant, i.e., 1000 W/m^{2}during

3s to 4.5 s. The temperature T_{solar} is maintained constant at 25 °Cduring 3s to 3.5s; then it is stepped from 25 °C to 50 °C at 3.5 s and maintained constant until 4 s; further, it is stepped down from 50 °C to 25 °C at 4 s and maintained constant until 4.5 s. Figure 15 shows the response of PV output power P_{PV}, PV terminal voltage V_{PV}, and current I_{PV} during3 s to 4.5 s with respect to change in environmental temperature T_{solar}. As like the response of PV output power P_{PV} seen in Figure 13, the PV system with the proposed HOA-chaos based MPPT controller extracted the maximum average power of 97.1976 kW during 3 s to 4.5 s, whereas the PV system with the P&O, INC, PSO, and HOA based MPPT controllers extracted merely 87.8406 kW, 89.8499 kW, 93.1014 kW, and 93.7312 kW, respectively as depicted in Table 4.

Figure 16 shows the response of load powerP_{Load}, load voltage V_{Load}, and load current I_{Load} during 3 s to 4.5 s with respect to change in temperature T_{solar}. As like the response of load power P_{Load} seen in Figure 14, the PV system with the proposed HOA-chaos based MPPT controller exported the maximum average power of 96.5193 kW to the load, whereas the PV system with the P&O, INC, PSO, and HOA based MPPT controllers exported 86.3925 kW, 88.7364 kW, 92.3743 kW, and 93.1199 kW, r respectively as shown in Table 4. Whenever the environmental temperature T_{solar} varies, the load powerP_{Load}, load voltage V_{Load}, and load current I_{Load} waveforms of the PV system with the presented P&O, INC, PSO, and HOA based MPPT controllers shown more oscillations. On the other hand, the PV system with the proposed HOA-chaos based MPPT controller reacted rapidly and settled with minimum oscillations.

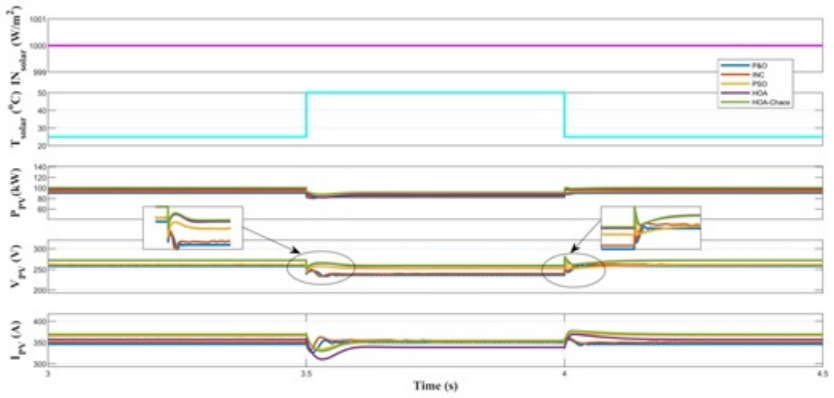

Figure 15: Scenario 2 – PV output powerP_{PV}, terminal voltageV_{PV}, and currentI_{PV}

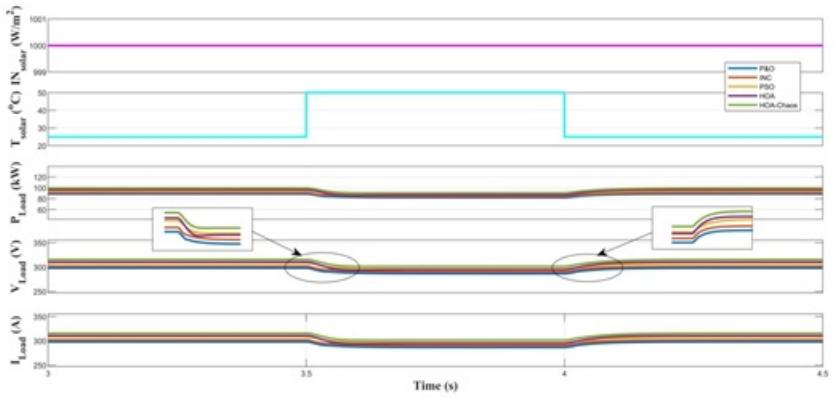

Figure 16: Scenario 2 – Load powerP_{Load}, voltageV_{Load}, and currentI_{Load}

Scenario 3 – Considering the simultaneous variation of solar insolation and temperature(t_{sim} = 4.5 s to 6 s)

In this simulation scenario, the solar insolation IN_{solar} falls on the PV array is considered as 1000 W/m^{2}during4.5 s to 5 s; then it is stepped down from 1000 W/m^2 to 800 W/m^2 at 5 s and maintained constant until 5.5 s; further, it is stepped up from 800 W/m^2 to 1000 W/m^2 at 5.5 s and maintained constant until 6 s. The temperature T_{solar} is maintained constant at 25 °Cduring4.5 s to 5 s and then it is stepped up from 25 °C to 50 °C at 5 s and maintained

constant until5.5 s; again, it is stepped down from 50 °C to 25 °C at 5.5 s and maintained constant until6 s. Figure 17 shows the response of power P_{PV} extracted from the PV array, PV terminal voltageV_{PV}, and current I_{PV}during4.5 s to 6 s with respect to change in solar insolation IN_{solar} and environmental temperatureT_{solar}. As like the response of PV power P_{PV}seen in Figures 13 and 15, the power waveform in Figure 17 depicts that the PV system with the proposed HOA-chaos based MPPT controller extracted the maximum average power of 90.2503 kWduring4.5 s to 6 s, whereas the PV system with the P&O, INC, PSO, and HOA based MPPT controllers extracted merely 81.4521 kW, 82.7162 kW, 85.2257 kW, and 87.7175 kW, respectively.

Figure 18 shows the response of load power P_{Load}, load voltage V_{Load}, and load current I_{Load} during4.5 s to 6 s with respect to simultaneous variation of solar insolationIN_{solar}, and temperatureT_{solar}. As like the response of load power P_{Load} seen in Figures 14 and 16, the PV system with the proposed HOA-chaos based MPPT controller exported the maximum average power of 89.6143 kW to the loadR_L, whereas the PV system with the P&O, INC, PSO, and HOA based MPPT controller exported 80.7888 kW, 82.3048 kW, 84.8715 kW, and 87.3235 kW, respectively as shown in Table 4. Whenever the solar insolation $IN_{solar}$and ambient temperature T_{solar}changes simultaneously, the load power P_{Load}, load voltage V_{Load}, and load current I_{Load} waveforms of the PV system with the P&O, INC, PSO, and HOA based MPPT controllers shown more oscillations. On the other side, the PV system with the proposed HOA-chaos based MPPT controller responded quickly and settled with very minimum oscillation.

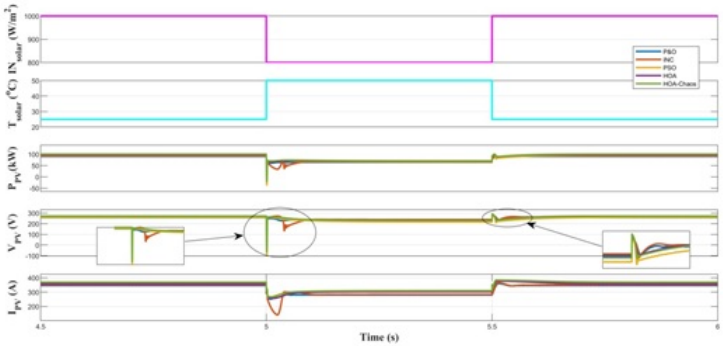

Figure 17: Scenario 3 - PV output power PPV, terminal voltage VPV, and current IPV

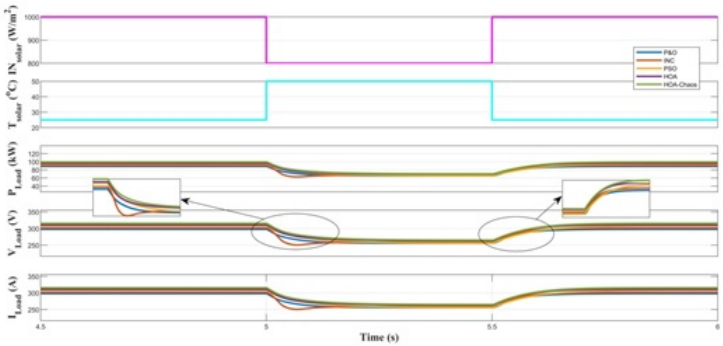

Figure 18: Scenario 3 – Load powerP_{Load}, voltageV_{Load}, and currentI_{Load}

6 Conclusion

To extract the most power from the PV array, a new, fast, and accurate MPPT controller called hurricane optimization algorithm hybridized with chaos based MPPT controller was developed. Its performance was validated under three different operating conditions,namely solar insolation variation, temperature variation, and simultaneous variation of both. The HOA-chaos algorithm has demonstrated an excellent capability to escape from the local maximum of MPOP, which frequently occurs due to the nonlinearity in the I–V characteristics of the PV array. The various case studies and the simulation results depicted that the proposed HOA-chaos based MPPT controller has provided a rigorous control and increased efficiency in terms of power extraction from the PV array. Furthermore,

the comparative findings revealed that the HOA-chaos based MPPT controller performed much better than theP&O, INC,PSO and HOA based MPPT controllers. By inserting the chaotic erotic dynamic steps into the standard HOA algorithm, the PV system with the proposed HOA-chaos based MPPT controller has brought good power conversion efficiency, utmost power extraction, and enhanced voltage response with less settling time, very minimum overshoot and undershoot. Therefore, the proposed HOA-chaos algorithm is a promising technique for the MPPT controller in the PV power generation system.

References

[1] K. Aseem and S.S. Kumar, *Hybrid k-means Grasshopper Optimization Algorithm based FOPID controller with feed forward DC–DC converter for solar-wind generating system*, J. Ambient Intell. Humaniz. Comput. (2021), https://doi.org/10.1007/s12652-021-03173-1.

[2] M. Benitez-Guerrero, B. Sarrion, A. Perejon, P.E. Sanchez-Jimenez, L.A. Perez-Maqueda and J. Manuel Valverde, *Large-scale high-temperature solar energy storage using natural minerals*, Sol. Energy Mater. Sol. Cells **168** (2017), 14–21.

[3] R. Foster and A. Cota, *Solar water pumping advances and comparative economics*, Energy Procedia **57** (2014), 1431–1436.

[4] J. Hyvarinen and J. Karila, *New analysis method for crystalline silicon cells*, Proc. 3rd World Conf. Photovoltaic Energy Conversion **2** (2003), 1521–1524.

[5] N.A. Kelly and T.L. Gibson,*Improved photovoltaic energy output for cloudy conditions with a solar tracking system*, Sol. Energy **83** (2009), no. 11, 2092–2102.

[6] Y. Lv, L. Xia, J. Yan and J. Bi, *Design of a hybrid fiber optic daylighting and PV solar lighting system*, Energy Procedia **145** (2018), 586–591.

[7] B. Liu, L. Wang, Y.-H. Jin, F. Tang and D.-X. Huang, *Improved particle swarm optimization combined with chaos*, Chaos Solitons Fractals **25** (2005), no. 5, 1261–1271.

[8] A. Loukriz, M. Haddadi and S. Messalti, *Simulation and experimental design of a new advanced variable step size incremental conductance MPPT algorithm for PV systems*, ISA Trans. **62** (2016), 30–38.

[9] L. Ma and Y. Lu, *Intelligent charging control method of shared vehicle based on MPPT algorithm in the environment of internet of things*, J. Ambient Intell. Humaniz. Comput. (2021), https://doi.org/10.1007/s12652-020-02812-3.

[10] R.P.K. Naidu and S. Meikandasivam, *Performance investigation of grid integrated photovoltaic/wind energy systems using ANFIS based hybrid MPPT controller*, J. Ambient Intell. Humaniz. Comput. **12** (2021), no. 5, 5147–5159.

[11] K. Nishioka, N. Sakitani, Y. Uraoka and T. Fuyuki, *Analysis of multicrystalline silicon solar cells by modified 3-diode equivalent circuit model taking leakage current through periphery into consideration*, Sol. Energy Mater. Sol. Cells **91** (2007), no. 13, 1222–1227.

[12] N. Pachaivannan, R. Subburam, M. Padmanaban and A. Subramanian, *Certain investigations of ANFIS assisted CPHO algorithm tuned MPPT controller for PV arrays under partial shading conditions*, J. Ambient Intell. Humanized Comput. **12** (2021), no. 10, 9923–9938.

[13] C. Parrado, A. Girard, F. Simon and E. Fuentealba, *LCOE (Levelized Cost of Energy) projection for a hybrid PV (photovoltaic)-CSP (concentrated solar power) plant in the Atacama Desert, Chile*, Energy **94** (2050), 422–430.

[14] L.M. Pecora and T.L. Carroll, *Synchronization in chaotic systems*, Phys. Rev. Lett. **64** (1990), no. 8, 821–824.

[15] L. Piegari and R. Rizzo, *Adaptive perturb and observe algorithm for photovoltaic maximum power point tracking*, IET Renew. Power Gener. **4** (2010), no. 4, 317–328.

[16] H. Rezk, A.O. Mazen, M.R. Gomaa, M.A. Tolba, A. Fathy, M.A. Abdelkareem, A.G. Olabi and M. Abou Hashema, *A novel statistical performance evaluation of most modern optimization-based global MPPT techniques for partially shaded PV system*, Renew. Sustain. Energy Rev. **115** (2019), 109372.

[17] I. Rbouh and A.A.E. Imrani, *Hurricane-based Optimization Algorithm*, AASRI Procedia **6** (2014), 26–33.

[18] I. Rbouh and A.A.E. Imrani, *Hurricane Search algorithm a new model for function optimization*, 5th Int. Conf. Inf. Commun. Syst. (ICICS), 2014, p. 1–5.

[19] R.M. Rizk-Allah, R.A. El-Sehiemy and G.-G. Wang, *A novel parallel hurricane optimization algorithm for secure emission/economic load dispatch solution* , Appl. Soft Comput. **63** (2018), 206–222.

[20] H.S. Rauschenbach, *Solar cell array design handbook: the principles and technology of photovoltaic energy conversion*, Springer Science and Business Media, 2012.

[21] S. Shongwe and M. Hanif, *Comparative analysis of different single-diode PV modeling methods*, IEEE J. Photovolt. **5** (2015), no. 3, 938–946.

[22] A. Subramanian and J. Raman, *Grasshopper optimization algorithm tuned maximum power point tracking for solar photovoltaic systems*, J. Ambient Intell. Humaniz. Comput. **12** (2021), no. 9, 8637–8645.

[23] M. Thirugnanasambandam, S. Iniyan, and R. Goic, *A review of solar thermal technologies*, Renew. Sustain. Energy Rev. **14** (2010), no. 1, 312–322.

[24] T. Tsoutsos, N. Frantzeskaki and V. Gekas, *Environmental impacts from the solar energy technologies*, Energy Policy **33** (2005), no. 3, 289–296.

[25] D. Yang, G. Li and G. Cheng, *On the efficiency of chaos optimization algorithms for global optimization*, Chaos Solitons Fractals **34** (2007), no. 4, 1366–1375.